analytical chemistry

Article

Cite This: Anal. Chem. 2018, 90, 3475−3481

pubs.acs.org/ac

Chemical Phenomena of Atomic Force Microscopy Scanning

Anton V. Ievlev,*[,†,‡] Chance Brown,[†,§] Matthew J. Burch,[†] Joshua C. Agar,[∥] Gabriel A. Velarde,[∥] Lane W. Martin,[∥,⊥] Petro Maksymovych,[†,‡] Sergei V. Kalinin,[†,‡] and Olga S. Ovchinnikova*[,†,‡]

[†]The Center for Nanophase Materials Sciences and [‡]Institute for Functional Imaging of Materials, Oak Ridge National Laboratory, 1 Bethel Valley Road, Oak Ridge, Tennessee 37831, United States

[§]The Bredesen Center, University of Tennessee, 821 Volunteer Boulevard, Knoxville, Tennessee 37920, United States

[∥]Department of Materials Science and Engineering, University of California Berkeley, Berkeley, California 94720, United States

[⊥]Materials Sciences Division, Lawrence Berkeley National Laboratory, Berkeley, California 94720, United States

Supporting Information

ABSTRACT: Atomic force microscopy is widely used for nanoscale characterization of materials by scientists worldwide. The long-held belief of ambient AFM is that the tip is generally chemically inert but can be functionalized with respect to the studied sample. This implies that basic imaging and scanning procedures do not affect surface and bulk chemistry of the studied sample. However, an in-depth study of the confined chemical processes taking place at the tip−surface junction and the associated chemical changes to the material surface have been missing as of now. Here, we used a hybrid system that combines time-of-flight secondary ion mass spectrometry with an atomic force microscopy to investigate the chemical interactions that take place at the tip−surface junction. Investigations showed that even basic contact mode AFM scanning is able to modify the surface of the studied sample. In particular, we found that the silicone oils deposited from the AFM tip into the scanned regions and spread to distances exceeding 15 μm from the tip. These oils were determined to come from standard gel boxes used for the storage of the tips. The explored phenomena are important for interpreting and understanding results of AFM mechanical and electrical studies relying on the state of the tip−surface junction.

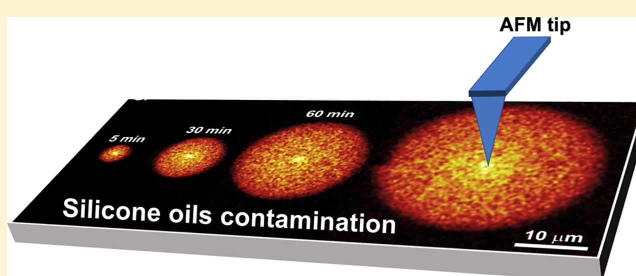

Since its invention approximately 30 years ago, atomic force microscopy (AFM) has become a cornerstone for functional material characterization at the nanoscale.[1] In the years following its invention, AFM has evolved from performing simple surface topographical measurements to advanced characterization that allows probing of mechanical, electrical, and magnetic phenomena with nanometer spatial resolution in a variety of environments relevant to material characterization such as vacuum, ambient, and even liquid.[2−14] Additionally, utilizing mechanical, electrical, and magnetic fields produced at the tip has also enabled AFM to be used as formidable lithographical technique.[15−17] For instance, mechanical pressure produced by the tip can be used to locally pattern soft matter, whereas electric fields produced by a biased tip can locally switch spontaneous polarization in ferroelectrics.[15,18−22] Overall, AFM's broad acceptance and utilization in functional imaging as well as lithography in diverse fields such biology, medicine, electrochemistry, and condensed matter physics come from it being considered nondestructive and nonaltering to the surface of the studied sample during imaging and its ability to serve for functional imaging and fabrication.[23−27]

The long-held belief of ambient AFM is that the tip is generally chemically inert but can be functionalized with respect to the studied sample. This implies that basic imaging and scanning procedures do not affect surface and bulk chemistry of the studied sample. However, an in-depth study of the confined chemical processes taking place at the tip−surface junction and the associated chemical changes to the material surface have been missing as of now. Therefore, interpretations of the functional response of the AFM tip with the surface in most cases ignore chemical contributions. However, if there are chemical changes that are unaccounted for, results from many AFM functional modes will be misinterpreted due to the unknown state of the tip/surface junction.

In this work, we used a hybrid system that combines the highly surface sensitive chemical analysis technique of time-of-flight secondary ion mass spectrometry (ToF-SIMS)[28,29] with an AFM in the same vacuum chamber to investigate the chemical interactions that take place at the AFM tip−surface junction. We used ToF-SIMS to study the local changes in chemical composition of the material surface when the AFM is operated in contact mode, which showed silicon (Si^+) deposition inside the scanned regions. The silicon was determined to come from uncross-linked small oligomers of polydimethylsiloxane (PDMS) that is used in standard gel boxes for the storage and transport of AFM chips. These

Received: December 14, 2017
Accepted: January 30, 2018
Published: January 30, 2018

Downloaded via UNIV OF CALIFORNIA BERKELEY on April 6, 2020 at 21:17:36 (UTC).
See https://pubs.acs.org/sharingguidelines for options on how to legitimately share published articles.

ACS Publications © 2018 American Chemical Society

DOI: 10.1021/acs.analchem.7b05225
Anal. Chem. 2018, 90, 3475−3481

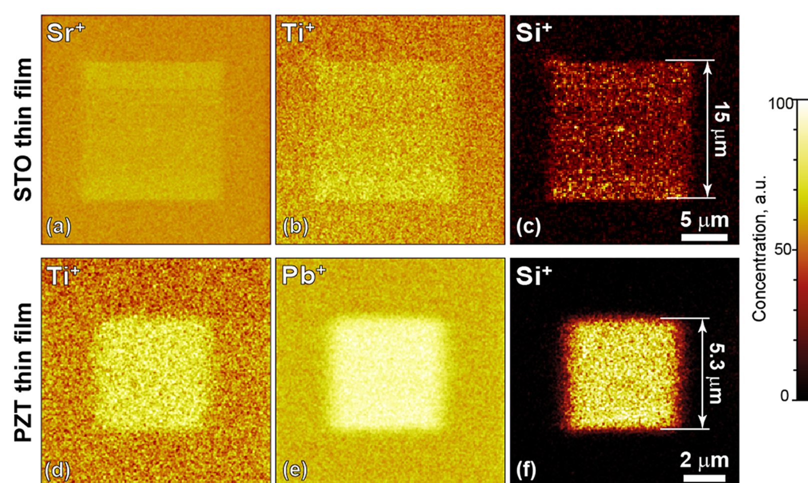

Figure 1. ToF-SIMS investigations of STO (a−c) and PZT (d−f) films scanned in contact AFM mode using the nanosensor PPP-EFM silicon tip with platinum−iridium coating. Maps of spatial distribution of Sr^+ (a), Ti^+ (b), and Si^+ (c) on the surface of STO and Ti^+ (d), Pb^+ (e), and Si^+ (f) on the surface of PZT.

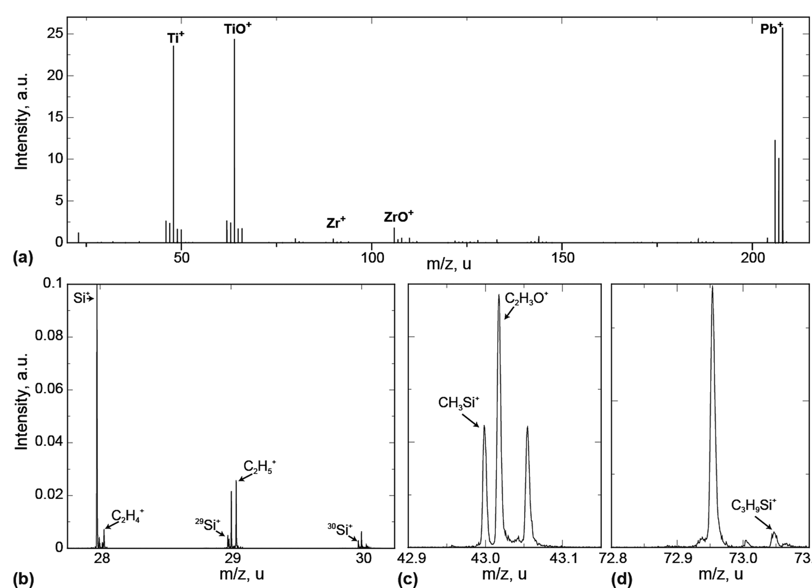

Figure 2. High spectra resolution ToF-SIMS investigations of the PZT surface after scanning with an AFM tip. (a) Total ion mass spectrum; (b−d) zoomed-in plots of (b) Si^+ isotopes, (c) CH_3Si^+, and (d) $C_3H_9Si^+$ peaks.

oligomers were observed to spread over the surface to distances exceeding 15 μm from the tip. The observed phenomenon was found to be universal for both studied sample and type of AFM tip, including fully metallic tips. The rates of the silicon deposition were found to be independent of contact force and electrical bias applied to the tip but dependent on the overall tip dwell time in contact with sample surface. The rates of silicone oils spread from the tip were also found to be linear with the time. Helium ion microscopy (HIM) and ToF-SIMS investigations of the tips showed that thin silicone oil contamination film could easily be removed with ion irradiation/sputtering. These results are fundamental for interpreting and understanding results of AFM studies used for functional characterization of materials.

■ EXPERIMENT AND RESULTS

The investigations of chemical interaction between the AFM tip and the surface of the studied sample were carried out using the TOF.SIMS.5-NSC (ION-TOF GmbH, Germany) instrument, which combines AFM and ToF-SIMS in the same vacuum chamber. For the measurements we used samples of strontium titanate ($SrTiO_3$, STO) and lead zirconate titanate $PbZr_{0.2}Ti_{0.8}O_3$ (PZT) thin films. The experiments were carried out in three stages: (1) The sample surface was cleaned using an O_2^- ion gun[30] to minimize the influence of the adsorption layers and surface contamination found on any surface that has been in ambient conditions. (2) The cleaned surface of the sample was scanned using AFM contact mode with detection of the surface topography. For scanning we used two types of silicon tips: nanosensors PPP-EFM with a platinum−iridium coating and NT-MDT DCP-01 with a diamond-like coating and one type of fully metallic platinum−iridium tip: RMN 25PtIr300B. (3) Finally, the scanned regions were studied by ToF-SIMS to detect changes of surface chemistry induced by the scanning. ToF-SIMS measurements were performed using positive-ion mode detection using a bismuth ion primary gun. ToF-SIMS imaging experiments were carried out with spatial resolution of ∼120 nm and spectral resolution of ∼0.3−0.5 Da.

DOI: 10.1021/acs.analchem.7b05225
Anal. Chem. 2018, 90, 3475−3481

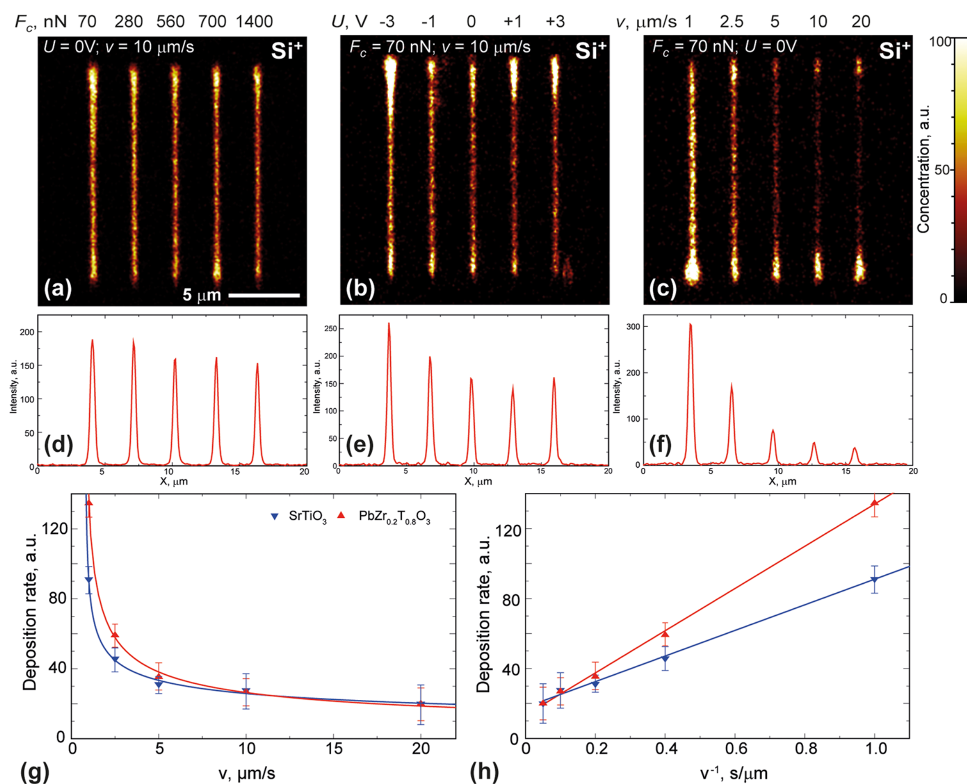

Figure 3. Silicon deposition on surface of PZT film during the scanning along lines with variation of scanning properties. (a−c) Chemical maps of silicon; (d−f) *x*-profiles of the silicon concentration. Variation of (a, d) contact force, (b, e) electrical bias applied to the tip, and (c, f) scanning speed. (g, h) Deposition rate versus scanning speed (g) and dwell time (h). Nanosensor silicon tip with platinum−iridium coating.

The results for STO thin film are presented in Figure 1a−c. Here, the 15 × 15 μm^2 region was scanned in contact mode using the nanosensor silicon tip with platinum−iridium coating. The averaged mass spectrum shows the prevalence of the peaks corresponding to base STO chemical elements (Sr^+ and Ti^+), as well as their oxides (Supporting Information, Figure S1a), which confirms the efficiency of the cleaning procedure with the O_2^- ion gun. Further, analysis of the chemical maps demonstrates a slight increase in the concentrations of Sr^+ and Ti^+ upon scanning (Figure 1a and b).

To understand the observed changes in surface chemical composition, we quantified the mass spectra in detail. We noted the presence of a significant amount of the silicon (Si^+), which was localized only inside the region scanned by AFM (Figure 1c). A similar phenomenon observed for silicon deposition from the AFM tip was found while scanning the surface of a PZT thin film and indium tin oxide (ITO)-coated glass (Figure 1d−f and Figures S1 and S2). These results demonstrate that the observed phenomenon is universal with respect to the studied sample.

To understand the source of the Si^+ signal, we further performed ToF-SIMS investigations with high spectral resolution. In this mode, the bismuth ion beam is intentionally slightly defocused, which provides for a spatial resolution of ∼5 μm but a much higher spectral resolution (<0.01 Da), allowing differentiation of isobaric overlaps between elements and molecular species with similar masses. In particular, this mode allowed us to separate out the silicon isotopes ($^{29}Si^+$ and $^{30}Si^+$) from the hydrocarbon background peaks (Figure 2a and b). The measured isotope peak abundancies showed the ratio characteristic to natural isotopic composition of silicon.[31] This confirmed that the contamination layer deposited by the tip during scanning actually contains silicon. However, this does not mean that the deposited silicon comes in a pure form. In fact, the presence of Si^+ can be detected in ToF-SIMS due to the fragmentation of a larger silicone-containing molecules. Therefore, we utilized the mass resolving power of the mass spectrometer to identify larger molecular fragments containing silicon. This analysis showed the presence of characteristic siloxane peaks CH_3Si^+ and $C_3H_9Si^+$, which were also localized inside the scanned region (Figure 2c and d).

The obtained results further explain the observed enhancement in the concentration of the base STO and PZT elements within the scanned square (Figure 1a, b, d, and e). In this case, the deposited silicon plays the role of matrix deposited on the surface of the studied sample, which enhances the generation of the secondary ions during ToF-SIMS studies.[32]

To further ascertain the mechanism for the silicon deposition on the sample surface, we investigated silicon deposition along the scan lines on the surface of PZT as a function of different scan parameters. In these measurements the scanning was carried out along single lines, with each line scanned twice (trace and retrace). As expected, the subsequent ToF-SIMS imaging demonstrated silicon localization along the lines (Figure 3a−c). The termini of the lines showed slightly elevated silicon concentrations, which was related to technicalities of the used scanning procedure (tip waited at the terminus for the coordinates of the next motion).

To study the deposition process we varied the contact force, electrical bias, and scanning speed along the lines. The contact force F_c ranged from 70 nN to 1.4 μN and did not show any influence on the deposition process (Figure 3a and d). Measurements with smaller values of F_c down to 10 nN showed the same results. Similarly, application of an electrical

DOI: 10.1021/acs.analchem.7b05225
Anal. Chem. 2018, 90, 3475−3481

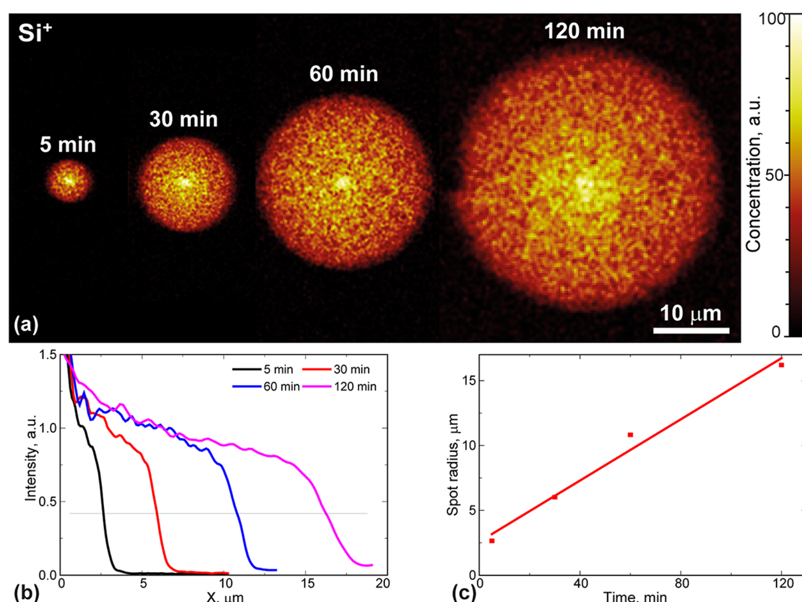

Figure 4. Silicon spread from stationary AFM tip. (a) Chemical maps of silicon distribution after dwell time of 5−120 min, as specified on the graph; (b) polar Si^+ profiles of averaged over silicon spots; (c) spot radius versus dwell time. PZT thin film. Nanosensor silicon tip with platinum−iridium coating.

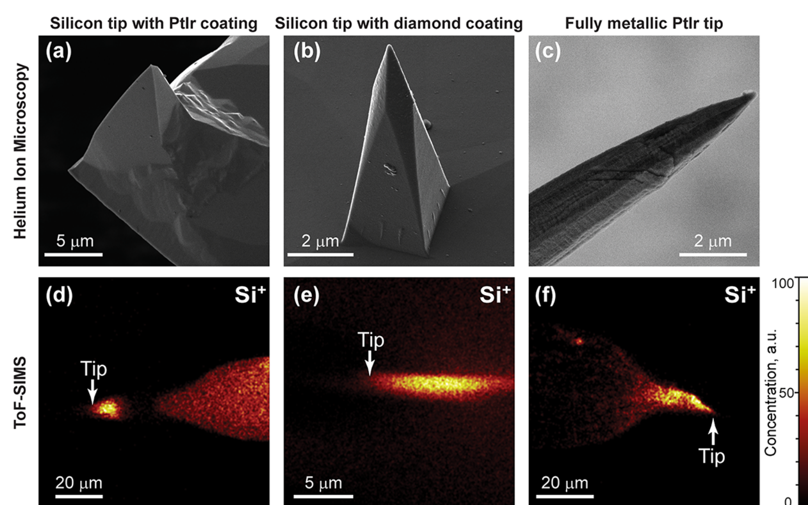

Figure 5. HIM and ToF-SIMS imaging of fresh, unused AFM tips. (a−c) HIM images of the tip morphology; (d−f) chemical maps of silicon distribution on the tip surface. (a, d) Nanosensor PPP-EFM silicon tip with PtIr coating; (b, e) NT-MDT DCP-01 silicon tip with diamond-like coating; (c, f) RMN 25PtIr300B fully metallic PtIr tip.

bias U = −3 to +3 V to the tip did not show any significant changes to the deposition rates (Figure 3b and e). However, scanning speed v was found to be the most important scanning parameter. The deposition rate was found to decrease with increasing scan speed (Figure 3c and f). Similar results were obtained while studying silicon deposition along the lines on the surface of STO thin films (Figure S3).

To understand these results we plotted the deposition rates as a function of scanning speed and inverted scanning speed (Figure 3g and h). Both plots showed similar shapes for PZT and STO films. PZT demonstrated much higher absolute values of the deposition rates, which may be related to electrostatic interaction of the deposited material with polarization in PZT, as well as matrix suppression and enhancement effects that come from using different substrates. Graphs plotted as a function of inverse speed (or dwell time) were found to be linear (Figure 3h); this means that deposition rate is constant over time.

Further, detailed studies also demonstrated that silicon can spread beyond the scanned regions. In the case of square scans, this led to formation of the circular halo around the scanned square with a smaller silicon concentration (Figure S4). To study this process systematically, we investigated silicon spread from a stationary tip sitting on the sample surface. Here, we varied the dwell time the tip remained on the surface from 5 to 120 min. In all cases, the results showed the formation of circular silicon footprints with a well-localized front (Figure 4a). The spot radius was found to increase with dwell time. The concentration profiles along the spots showed the maximum silicon concentration right underneath the tip and an abrupt drop at the front, while in between the concentration changed insignificantly (Figure 4b). Stable silicon concentration within the spot as well as a well-localized front can be explained by the

DOI: 10.1021/acs.analchem.7b05225
Anal. Chem. 2018, 90, 3475−3481

spread of a silicon monolayer. The spot radius was found to be linear with respect to the dwell time (Figure 4c). Obtained results cannot be described by a simple diffusional model, as in the case of diffusional spread spot size is expected to be proportional to square root of the time. Furthermore, the diffusional model contradicts with concentration profile within the deposited spot (Figure 4b). Thereby, additional phenomena (e.g., gravity and surface tension) need to be taken into account to model deposition of the silicone oils from the tip.

To understand the origin of the silicon deposited on the sample surface, we performed experiments with different types of AFM tips. We used two types of silicon tips with platinum−iridium and diamond-like coatings as well as one type of fully metallic platinum−iridium tip. Surprisingly, we found silicon deposition from all tips (Figure S5). We expected to see such a result for first two tip types, as those tips are made of silicon. However, the fact that even fully metallic tips are capable of silicon deposition is nontrivial. To understand this process, we performed characterization of the tips morphology using a HIM (Figure 5a−c) and their chemical composition using ToF-SIMS (Figure 5d−f). Chemical imaging showed that the surface of all the tips is heavily contaminated by the silicon. Concentration of silicone oils was found to be higher at the tip apex. This fact can be attributed to silicone oils concentration near the tip apex due to its geometry. However, it can be also a technical effect, caused by the different values of the sputter yields at differently oriented parts of cantilever and tip. We also found that contamination could be cleaned or sputtered with continuous exposure to helium ion irradiation in the HIM or bismuth ions in ToF-SIMS (Figure 6). Additional HIM images of used AFM tips can be found in Figure S6.

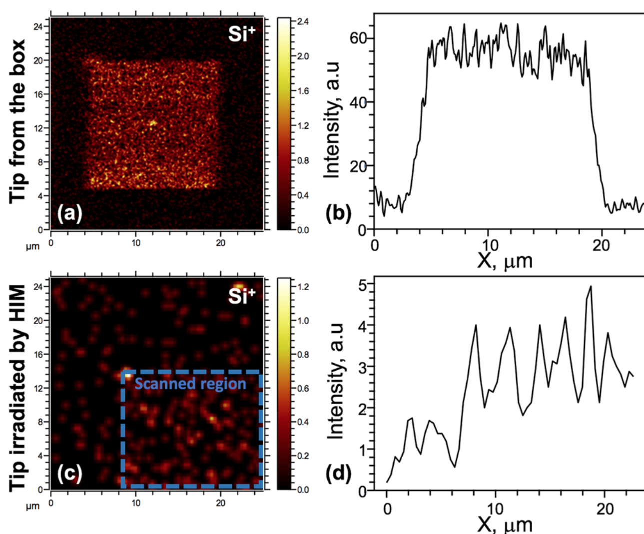

Figure 6. ToF-SIMS investigations of STO surface by fresh AFM tip from the box (a, b) and tip irradiated by helium ion microscope (c, d). Chemical maps of silicon distribution (a, c) and X-profiles averaged over scanned region (b, d). Nanosensor silicon tip with platinum−iridium coating.

These results help to explain silicon deposition from a fully metallic tip. Deposition is driven not by the silicon from the tip composition but from the thin contamination layer covering the apex of the tip. This is in good agreement with the study published in 1999, which showed contamination of commercial AFM tips by silicone oils.[33] Observed contamination most likely stems from the polydimethylsiloxane (PDMS) gel boxes, which are widely used for the storage of AFM tips. It has been shown that PDMS can contain a significant amount of uncross-linked oligomers (or silicone oils) with low molecular masses,[34,35] which can diffuse over the surface of different materials.[36] In our case the deposition of silicone oils onto the surface is mostly independent of the tip chemical composition or properties but dependent on conditions in which the tip was stored prior to the measurements. PDMS oligomer contamination of the AFM tips is also confirmed by existence of characteristic siloxane peaks of CH_3Si^+ and $C_3H_9Si^+$ inside the scanned regions (Figure 2c and d).

The phenomena revealed here are important for interpreting and understanding characterization of the material properties by AFM, which relies on the tip−surface interaction. Experiments also showed that contamination is possible when measurements are performed in tapping-mode AFM (Figure S7), which is widely used to study biological samples and soft matter. It has also been demonstrated that such a type of contamination is present in ambient AFM measurements. In this case AFM scanning of the PZT surface was realized using ambient AFM and the sample surface was further examined in vacuum using ToF-SIMS. These measurements clearly showed deposition of the silicon oils inside the scanned regions (Figure S8). These results demonstrate that basic AFM scanning can significantly change the properties of the studied sample, by changing the mechanical, electrical, and electrochemical response of the AFM tip to the surface. Unfortunately, ToF-SIMS measurements do not allow one to quantify the amount of the deposited material, as sputter yield can be significantly different for different chemical species. We can only speculate that the amount of deposited silicone oils is insignificant, as it cannot be clearly identified in subsequent AFM scanning.

Therefore, to get accurate and quantitative results when performing functional AFM measurements, tips need to be cleaned prior to the measurement. As an example, low-dose ion sputtering was shown to be effective at removing the siloxane contamination on the AFM tips. Our experiments showed that silicon deposition rate from the tips imaged using the HIM was 10 times smaller than that for the fresh tips from the gel box, which we attribute to sputtering of the contamination silicone oils by the helium ions during HIM imaging (Figure 6).

■ CONCLUSIONS

In this work, we explored the nanoscale chemical interaction that takes place during contact scanning by AFM using a novel hybrid system that combines ToF-SIMS with AFM in the same vacuum chamber. Our results showed that the commercial AFM tips are heavily contaminated by silicone oils, which can be deposited on the surface of a studied sample during AFM scanning. After being deposited on the surface, the silicone oils were found to spread on the surface to distances exceeding 15 μm from the tip. Further, investigations revealed that this phenomenon is universal for different samples and different tip types, including fully metallic tips. Deposition and spread rates were found to be linearly dependent on the tip dwell time in contact with the sample surface. Additionally, we found that ion irradiation can be used to remove silicone oil contamination form the tip and decrease the deposition rates by an order of magnitude. The obtained results point to the importance of understanding and interpretation of chemical tip effects in the quantitative characterization of materials using AFM.

DOI: 10.1021/acs.analchem.7b05225
Anal. Chem. 2018, 90, 3475−3481

METHODS

Atomic Force Microscopy. Atomic force microscopy measurements have been carried out using Nanoscan AFM instrument introduced into the ToF-SIMS vacuum chamber. Scanning was performed using three types of AFM tips: (1) nanosensor PPP-EFM silicon tip with platinum–iridium coating; (2) NT-MDT DCP-01 silicon tips with diamond-like coating; (3) RMN 25PtIr300B fully metallic platinum–iridium tips. Scanning was performed in contact mode with contact force F_c varied from 70 nN to 1.4 μN, electrical bias applied to the tip $U = -5$ to $+5$ V, and scanning speed v that ranged from 1 to 20 μm/s. All measurements have been done in vacuum, 5–8 $\times$ 10^{-9} mbar.

Time-of-Flight Secondary Ion Mass Spectrometry. ToF-SIMS measurements have been done using TOF.-SIMS.5-NSC instrument, using bismuth ion gun as a primary ion source and O_2^- ion gun as a sputter source. For the imaging ToF-SIMS experiments, we used mode with high spatial resolution, Bi spot size ∼120 nm, energy 30 keV, current 0.48 nA, and spectral resolution 0.3–0.5 Da. High spectral resolution mode was also used to identify mass peaks of the deposited silica. In this mode we used Bi spot size ∼5 μm, energy 30 keV, current 30 nA, and spectral resolution <0.01 Da.

Sputter O_2^- ion gun (energy 1 keV, current 120 nA, and spot size ∼20 μm) was used for surface cleaning of the samples before experiments. The cleaning was performed over an area of 300 × 300 μm under the control of ToF-SIMS in noninterlaced mode. In this mode, each sputtering step of 2 s was followed by analysis of surface chemical composition by bismuth primary source. The procedure was repeated until contamination peaks were minimized in comparison with peaks of the studied sample.

Helium Ion Microscopy. Helium ion microscopy images of the AFM tips were obtained on a Zeiss Orion Nanofab after being mounted onto carbon tape for imaging. For imaging, an accelerating of 25 keV, a 10 μm Au aperture, and beam currents of ∼1.5 pA were used.

ASSOCIATED CONTENT

Supporting Information

The Supporting Information is available free of charge on the ACS Publications website at DOI: 10.1021/acs.analchem.7b05225.

Averaged mass spectra on the surface of PZT and STO thin films, silicon oils contamination of the surface of ITO-coated glass, silicon deposition during the scanning along lines on the surface of the STO, silicon spread outside scanned regions, silicon oils contamination by different types of AFM tips, helium ion microscopy images of the AFM tips, silicone oil contamination during scanning in tapping AFM mode, silicone oil contamination during enviromental AFM measurements (PDF)

AUTHOR INFORMATION

Corresponding Authors

*E-mail: ievlevav@ornl.gov.

*E-mail: ovchinnikovo@ornl.gov.

ORCID

Anton V. Ievlev: 0000-0003-3645-0508

Matthew J. Burch: 0000-0001-6139-9404

Lane W. Martin: 0000-0003-1889-2513

Olga S. Ovchinnikova: 0000-0001-8935-2309

Notes

This manuscript has been authored by UT-Battelle, LLC, under Contract No. DE-AC0500OR22725 with the U.S. Department of Energy. The United States Government retains and the publisher, by accepting the article for publication, acknowledges that the United States Government retains a nonexclusive, paid-up, irrevocable, worldwide license to publish or reproduce the published form of this manuscript, or allow others to do so, for the United States Government purposes. The Department of Energy will provide public access to these results of federally sponsored research in accordance with the DOE Public Access Plan (http://energy.gov/downloads/doe-public-access-plan).

The authors declare no competing financial interest.

ACKNOWLEDGMENTS

This material is based upon work supported by the U.S. Department of Energy, Office of Science, Office of Basic Energy Sciences, under Contract no. DE-AC05-00OR22725 by the Laboratory Directed Research and Development Program of Oak Ridge National Laboratory, managed by UT-Battelle, LLC, for the U.S. Department of Energy (AVI, OSO). ToF-SIMS and AFM measurements were performed at the Center for Nanophase Materials Sciences, which is a DOE Office of Science User Facility. J.C.A. acknowledges support from the Army Research Office under Grant W911NF-14-1-0104. G.A.V. acknowledges support from the National Science Foundation under Grant DMR-1708615. L.W.M. acknowledges support from the National Science Foundation under Grant DMR-1608938.

REFERENCES

(1) Binnig, G.; Quate, C. F.; Gerber, C. *Phys. Rev. Lett.* **1986**, *56*, 930–933.
(2) Majumdar, A. *Annu. Rev. Mater. Sci.* **1999**, *29*, 505–585.
(3) Sidles, J. A.; Garbini, J. L.; Bruland, K. J.; Rugar, D.; Zuger, O.; Hoen, S.; Yannoni, C. S. *Rev. Mod. Phys.* **1995**, *67*, 249–265.
(4) Nonnenmacher, M.; O'Boyle, M. P.; Wickramasinghe, H. K. *Appl. Phys. Lett.* **1991**, *58*, 2921–2923.
(5) Nonnenmacher, M.; Wickramasinghe, H. K. *Appl. Phys. Lett.* **1992**, *61*, 168–170.
(6) Kalinin, S. V.; Morozovska, A. N.; Chen, L. Q.; Rodriguez, B. J. *Rep. Prog. Phys.* **2010**, *73*, 056502.
(7) Soergel, E. *J. Phys. D: Appl. Phys.* **2011**, *44*, 464003.
(8) Hartmann, U. *Annu. Rev. Mater. Sci.* **1999**, *29*, 53–87.
(9) Matey, J. R.; Blanc, J. *J. Appl. Phys.* **1985**, *57*, 1437–1444.
(10) Rabe, U.; Arnold, W. *Appl. Phys. Lett.* **1994**, *64*, 1493–1495.
(11) Hong, S.; Tong, S.; Park, W. I.; Hiranaga, Y.; Cho, Y. S.; Roelofs, A. *Proc. Natl. Acad. Sci. U. S. A.* **2014**, *111*, 6566–6569.
(12) Jesse, S.; Baddorf, A. P.; Kalinin, S. V. *Appl. Phys. Lett.* **2006**, *88*, 062908.
(13) Ko, H.; Ryu, K.; Park, H.; Park, C.; Jeon, D.; Kim, Y. K.; Jung, J.; Min, D. K.; Kim, Y.; Lee, H. N.; Park, Y.; Shin, H.; Hong, S. *Nano Lett.* **2011**, *11*, 1428–1433.
(14) Kim, H.; Hong, S.; Kim, D. W. *Appl. Phys. Lett.* **2012**, *100*, 022901.
(15) Cho, Y.; Fujimoto, K.; Hiranaga, Y.; Wagatsuma, Y.; Onoe, A.; Terabe, K.; Kitamura, K. *Appl. Phys. Lett.* **2002**, *81*, 4401.
(16) Ievlev, A. V.; Morozovska, A. N.; Shur, V. Y.; Kalinin, S. V. *Phys. Rev. B: Condens. Matter Mater. Phys.* **2015**, *91*, 214109.
(17) Garcia, R.; Calleja, M.; Perez-Murano, F. *Appl. Phys. Lett.* **1998**, *72*, 2295–2297.
(18) Paruch, P.; Tybell, T.; Triscone, J. M. *Appl. Phys. Lett.* **2001**, *79*, 530.

(19) Terabe, K.; Takekawa, S.; Nakamura, M.; Kitamura, K.; Higuchi, S.; Gotoh, Y.; Gruverman, A. *Appl. Phys. Lett.* **2002**, *81*, 2044.
(20) Agronin, A.; Molotskii, M.; Rosenwaks, Y.; Rosenman, G.; Rodriguez, B. J.; Kingon, A. I.; Gruverman, A. *J. Appl. Phys.* **2006**, *99*, 104102.
(21) Shishkin, E. I.; Ievlev, A. V.; Nikolaeva, E. V.; Nebogatikov, M. S.; Shur, V. Y. *Ferroelectrics* **2008**, *374*, 26−32.
(22) Choi, Y. Y.; Sharma, P.; Phatak, C.; Gosztola, D. J.; Liu, Y. Y.; Lee, J.; Lee, B.; Li, J. Y.; Gruverman, A.; Ducharme, S.; Hong, S. *ACS Nano* **2015**, *9*, 1809−1819.
(23) Rugar, D.; Budakian, R.; Mamin, H. J.; Chui, B. W. *Nature* **2004**, *430*, 329−332.
(24) Ievlev, A. V.; Jesse, S.; Morozovska, A. N.; Strelcov, E.; Eliseev, E. A.; Pershin, Y. V.; Kumar, A.; Shur, V. Y.; Kalinin, S. V. *Nat. Phys.* **2014**, *10*, 59−66.
(25) Rabe, U.; Amelio, S.; Kopycinska, M.; Hirsekorn, S.; Kempf, M.; Goken, M.; Arnold, W. *Surf. Interface Anal.* **2002**, *33*, 65−70.
(26) Shi, L.; Zhou, J. H.; Kim, P.; Bachtold, A.; Majumdar, A.; McEuen, P. L. *J. Appl. Phys.* **2009**, *105*, 104306.
(27) Tong, S.; Jung, I. W.; Choi, Y. Y.; Hong, S.; Roelofs, A. *ACS Nano* **2016**, *10*, 2568−2574.
(28) McDonnell, L. A.; Heeren, R. M. A. *Mass Spectrom. Rev.* **2007**, *26*, 606−643.
(29) Ievlev, A. V.; Maksymovych, P.; Trassin, M.; Seidel, J.; Ramesh, R.; Kalinin, S. V.; Ovchinnikova, O. S. *ACS Appl. Mater. Interfaces* **2016**, *8*, 29588−29593.
(30) Ievlev, A. V.; Chyasnavichyus, M.; Leonard, D.; Agar, J. C.; Velarde, G. A.; Martin, L. W.; Kalinin, S. V.; Maksymovych, P.; Ovchinnikova, O. S. *Nanotechnology* **2018**, DOI: 10.1088/1361-6528/aaac9b.
(31) Vocke, R. D. *Pure Appl. Chem.* **1999**, *71*, 1593−1607.
(32) Smentkowski, V. S. *J. Vac. Sci. Technol., A* **2015**, *33*, 05E107.
(33) Lo, Y. S.; Huefner, N. D.; Chan, W. S.; Dryden, P.; Hagenhoff, B.; Beebe, T. P. *Langmuir* **1999**, *15*, 6522−6526.
(34) Regehr, K. J.; Domenech, M.; Koepsel, J. T.; Carver, K. C.; Ellison-Zelski, S. J.; Murphy, W. L.; Schuler, L. A.; Alarid, E. T.; Beebe, D. J. *Lab Chip* **2009**, *9*, 2132−2139.
(35) Millet, L. J.; Stewart, M. E.; Sweedler, J. V.; Nuzzo, R. G.; Gillette, M. U. *Lab Chip* **2007**, *7*, 987−994.
(36) Yunus, S.; de Looringhe, C. D.; Poleunis, C.; Delcorte, A. *Surf. Interface Anal.* **2007**, *39*, 922−925.

DOI: 10.1021/acs.analchem.7b05225
Anal. Chem. 2018, 90, 3475−3481